Michigan Technological University

Digital Commons @ Michigan Tech

Michigan Tech Publications

2021

Effect of Spectral Bandwidths on Linear Feature Extraction: An Evaluation of Landsat ETM+ and OLI Sensors

Ali Imanian
Shiraz University

Adel Asadi
Michigan Technological University, aasadi@mtu.edu

Majid Hashemi Tangestani
Shiraz University

Saeid Homayouni
University of Ottawa

Ali Faghih
Shiraz University

Follow this and additional works at: https://digitalcommons.mtu.edu/michigantech-p

Part of the Geological Engineering Commons, and the Mining Engineering Commons

Recommended Citation

Follow this and additional works at: https://digitalcommons.mtu.edu/michigantech-p

Part of the Geological Engineering Commons, and the Mining Engineering Commons

PAPER • OPEN ACCESS

Effect of Spectral Bandwidths on Linear Feature Extraction: An Evaluation of Landsat ETM+ and OLI Sensors

View the article online for updates and enhancements.

Effect of Spectral Bandwidths on Linear Feature Extraction: An Evaluation of Landsat ETM+ and OLI Sensors

Ali Imanian [1], Adel Asadi [2*], Majid Hashemi Tangestani [1], Saeid Homayouni [3] and Ali Faghih [1]

[1] Department of Earth Sciences, College of Sciences, Shiraz University, Shiraz, Iran.

[2] Geological and Mining Engineering and Sciences Department, Michigan Technological University, 1400 Townsend Drive, Houghton, MI 49931, USA.

[3] Department of Geography, Environment and Geomatics, University of Ottawa, Ottawa, ON K1N 6N5, Canada.

[*] aasadi@mtu.edu

Abstract. Hitherto there have been many studies comparing the usefulness of OLI and ETM+ sensors for linear feature extraction. However, not too much attention has been paid to the differences in the bandwidth of the two sensors. In this study, the suitability of Landsat ETM+ and OLI sensors for automatic detection of linear features by LINE algorithm was compared. In this study, eight regions in northern, central and southern parts of Iran were selected based on the diversity of lithology, the pristine status, and lack of human activities for the comparison of the two datasets. Results revealed that LINE algorithm performed better on the images with higher standard deviation. The ETM+ datasets are more suitable for linear feature extraction because ETM+ panchromatic band and first principal component analysis image (PC1 image) of ETM+ datasets have higher standard deviation compared to OLI datasets.

1. Introduction

Detection and extraction of linear features using digital images such as satellite or aerial images is a very important low-level operation in computer vision which has several applications. For instance, satellite imagery can be used to extract roads, railroads, rivers and other targets, and can be applied for capturing or updating data for navigation systems or for production of basic geographic maps. Remote sensing as a powerful tool to obtain information from the surface of the earth has been used widely for this purpose. In recent decades, remote sensing techniques have made progress in the earth science studies by aiding in the identification of linear features [1-6]. Several methodologies have been developed for the extraction of linear features. These include Kalman filtering, dynamic programming, multi-scale grouping and context, fuzzy-based approach, model-based approach, mathematical morphology, and image fusion. LINE algorithm in the PCI Geomatica software is the most commonly used automatic approach for linear feature extraction [7-9]. This algorithm employs the Canny method and detects the edge in images in three consecutive stages, namely edge detection, thresholding and curve extraction [10]. This study aims to compare the suitability of Landsat 7's ETM+ and Landsat 8's OLI data for linear feature extraction using LINE algorithm in PCI Geomatica Software. For this purpose, the performance of LINE algorithm on panchromatic bands and PC1 images of these datasets

were compared. In contrast to the previous studies which have focused on the determination of the suitable bands or the best False Colour Composite (FCC) bands to detect linear features, this study considers the possible effect of bandwidth on the linear feature extraction. The count of detected linear features and the total length of linear features were used for comparing the performance of LINE algorithm on dataset pairs of ETM+ and OLI in each study area.

2. Study Area

The study areas were chosen to contain various lithological diversities, e.g., igneous, sedimentary, and metamorphic rocks. The study areas are located in various regions in Iran, near Tabriz, Mashhad, Yasuj, Shahr-E-Kord, Yazd, Rafsanjan, Larestan, and Iranshahr cities. Yazd and Shahrekord cities are located in central Iranian block. This block is one of the most complicated structural zones in Iran. In this zone, rocks are deformed by several orogenic episodes, and metamorphism and magmatism is abundant. Shahrekord city is located in the Sanandaj-Sirjan zone. A striking feature of this zone is the presence of immense volumes of magmatic and metamorphic rocks. Mashhad city is located in Kopet Dagh. No significant sedimentary gap or volcanic formations are reported in this zone, and their sedimentary rocks were placed in their current position due to the uplift of the crust. Iran-Shahr city is located in the Makran zone and contains the ophiolites overlain by a thick sequence of sandstone, shale, and marl about 5,000 m thick [11-14]. Figure 1 shows the locations of the study areas on the structural map of Iran.
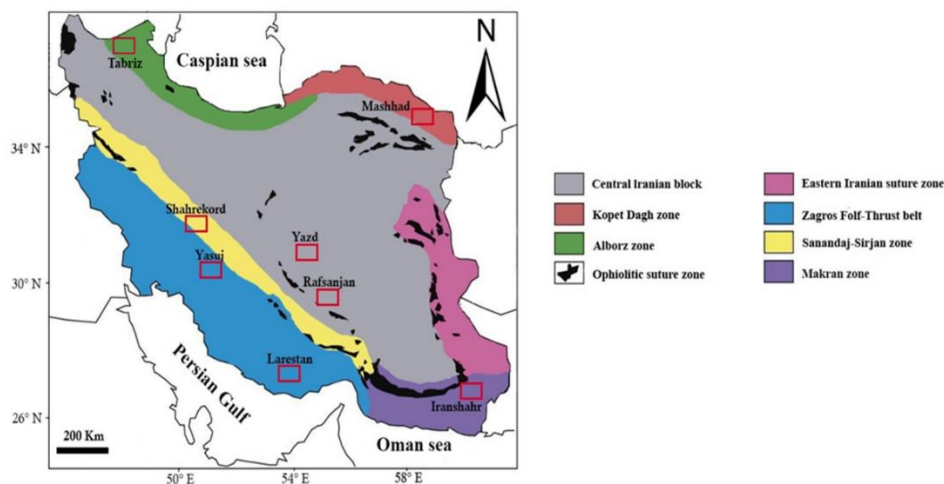
Figure 1. Location of the study areas on the structural zone of Iran, modified after Shafaii Moghadam and Stern (2014).

3. Materials and Methods

3.1. Remote Sensing Data

Enhanced Thematic Mapper Plus (ETM+) sensor onboard Landsat 7 satellite with a repeat cycle of 16 days was launched into space in July 1999. The Scan Line Corrector (SLC) instrument of the ETM+ sensor stopped working correctly in 2003, and consequently, the images collected by this sensor since May 30, 2003, have data gaps called SLC-off images. Operational Land Imager (OLI) is an instrument onboard Landsat 8 satellite, which was launched in February 2013. The spectral bands of the OLI sensor are similar to Landsat 7's ETM+ sensor except for two additional spectral bands. Band 1 is a deep blue visible channel designed for water resources and coastal zone observations, and band nine is designed for the detection of cirrus clouds. Similar to ETM+ data, Landsat 8's OLI data has 30-meters spatial resolution for bands 1 to 7 and band 9. Additionally, the band 8 is a panchromatic band with 15-meter spatial resolution. OLI scene size is approximately 170 km north-south by 183 km east-west similar to Landsat 7 data. The collection category of both ETM+ and OLI images used in this study are Tier 1 (T1). This category of Landsat satellite series is an inventory structure for Landsat Collection 1 Level-1 data products. These contain the highest quality Level 1 Precision Terrain (L1TP) data considered

suitable for time-series analysis. The geo-registration of Tier 1 data is consistent, with tolerances less than 12 meters root mean square error (RMSE). The datasets used in this study were collected in the time window of October 2002 to June 2017.

3.2. Image Analysis

The failure of SLC instrument of the ETM+ sensor caused a time gap between the perfect ETM+ images collected before 2003 and OLI data collected from 2013 onwards. Considering that the ETM+ data were collected fourteen years before that of the OLI, to eliminate the effects of human artifacts like pipelines, railways, and roads on image comparison of the two datasets, relatively pristine areas devoid of human activities were chosen as areas of study. Figure 2 shows the pristine nature of the study area around Yasuj and Mashhad cities.
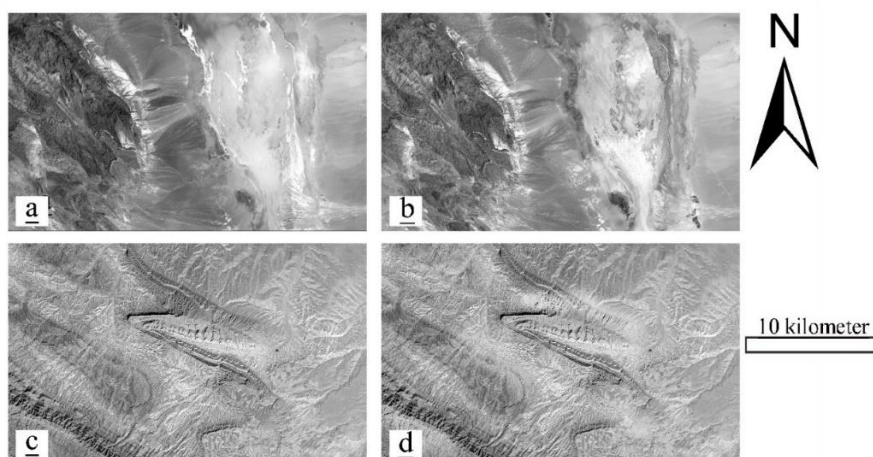
Figure 2. Panchromatic bands of two of selected study areas: a) ETM+ image acquired in October 17'th 2002; b) OLI image acquired in October 19'th 2016 around the Yasuj city; c) ETM+ image acquired in October 25'th 2002; d) OLI image acquired in October 23'th 2016 around Mashhad city.

One of the factors affecting linear feature extraction is the angle of solar radiation [15]. The change of radiation angle changes the length of shadows. Since the images of Landsat 7 and 8 were taken at the same time in Iran, this parameter did not have a considerable effect on image pair comparison. To prepare the datasets for comparison, the digital numbers (DNs) were converted to radiance using Equation (1).

$$L_\lambda = M_{\mathrm{L}} * Q_{cal} + A_{\mathrm{L}} \tag{1}$$

Where, L_λ is spectral radiance (W/(m^2*sr*μm)), M_{L} is radiance multiplicative scaling factor for the band, Q_{cal} is pixel's value in DN and A_{L} is radiance additive scaling factor for the band. Afterwards, radiance data was corrected to the surface reflectance using the Dark Object Subtraction method (DOS) [16-18]. Because multispectral data are often highly correlated, Principal Components Analysis was used to produces uncorrelated output bands to segregate noise components and to reduce the dimensionality of datasets [19,20]. To obtain the PC1 image bands 1 to 5, and 7 of ETM+ and bands 1 to 7 and 9 of OLI sensor were used. The suitability of PC1 of ETM+ dataset was compared to PC1 image of OLI dataset in each study area. Likewise, the panchromatic band of ETM+ dataset was compared with the panchromatic band of OLI. To determine the superiority of each dataset, the total length and number of detected linear features were compared to each other. Linear features were detected by LINE algorithm using PCI Geomatica software. This algorithm needs six input parameters and executes in three consecutive steps, namely edge detection, thresholding, and curve extraction. The LINE algorithm primarily operates on a single 8-bit image channel. If the input image is not in 8 bits, the image is first converted to an 8-bit image using a nonlinear scaling function. To consider the effect of this conversion on the LINE algorithm, all of the OLI images that were initially in 16-bit depth were also converted to 8-bit data manually before using LINE algorithm. For the manual conversion of 16-bit images to 8-bit

images, both nonlinear logarithmic function and linear function were used. The linear function rescales the highest value of 16-bit data (corresponding to a DN of 2^16 -1 = 65535) to a value of 255 (2^8 - 1) and its lowest value to 0, and the values in between are scaled proportionately using Equation (2).

$$Q_{i.j} = \frac{DN_{ij}}{DN_{max}} * Q_{max} \qquad (2)$$

Where, $Q_{i,j}$ is the DN value after rescaling to 8 bits, DN_{ij} is the DN value of each pixel in 16-bit, DN_{max} is the maximum value in 16-bit depth (65535) and Q_{max} is the maximum value in 8-bit depth (255). The logarithmic function converts DN values to the logarithm in base 10 using Equation (3).

$$Q_{i.j} = c * log_{10}(1 + DN_{i.j}) \qquad (3)$$

Where, $Q_{i.j}$ is the re-scaled value from 16-bit to 8 bits, c is the scaling constant, and DN_{ij} is the value of each pixel in 16 bits. The logarithmic function will change the frequency chart of the DN values. In a logarithmic scale, variations of DNs of lower values are more pronounced than variations of pixels with higher DNs. Since the logarithm is not defined for 0, the value 1 must be added to the image before logarithmic conversion. The scaling constant c is chosen so that the maximum output value (Q_{max}) is 255. If DN_{max} is the maximum value in the input image, c is given by Equation (4).

$$c = \frac{Q_{max}}{log(1+ DN_{max})} \qquad (4)$$

The spectral bandwidth of the images and the standard deviation of images were compared to each other to find the relation between standard deviation, algorithm performance and bandwidth variations. Before computing the standard deviation of the images, the digital number values of all of the images were rescaled between 0 and 1 using Equation (5).

$$DN_{nor} = \frac{DN_i - DN_{min}}{DN_{max} - DN_{min}} \qquad (5)$$

Where DN_{nor} is the normalized value of digital number between 0 and 1, DN_i is digital number value of each pixel, DN_{min} and DN_{max} are minimum and maximum digital number values of the image. Figure 3 presents the proposed method for this comparison.
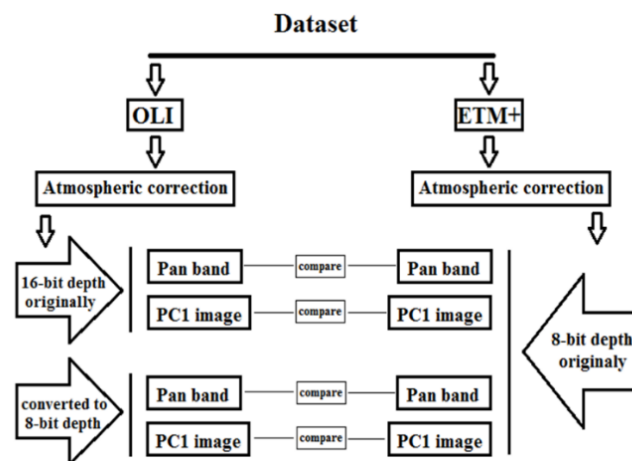
Figure 3. The method for comparison between ETM+ and OLI sensors for linear feature detection.

4. Results and Discussion

One of the most important parameters which affects the quality of satellite images is the signal-to-noise ratio (SNR). This phenomenon, which is caused by the electronic errors in the sensor's detectors, is an inevitable part of satellite systems imagery. In case of using satellite images to extract linear features, noises can be represented as short lines. Due to the possibility of occurrence of this error, the detected linear features which were shorter than the size of two pixels, were removed from results. The panchromatic bands of ETM+ and OLI sensors were given as an input to the LINE algorithm for linear feature detection without any prior conversion of OLI band to 8-bit data. The results of the operation on panchromatic bands for some study areas are given in Table 1. Considering the number and total length

of detected linear features, these results show that LINE algorithm performed better on ETM+ panchromatic bands compared to those of OLI in all study areas.

Table 1. Results of execution the LINE algorithm on the panchromatic bands of ETM+ (8-bit depth) and OLI (16-bit depth) datasets.

Field study	Data type	Number of segments	Sum of lengths (km)
Shahrekord	PAN _ ETM+	9604	9534
	PAN _ OLI	7306	6765
Tabriz	PAN _ ETM+	5046	5047
	PAN _ OLI	3908	3850
Larestan	PAN _ ETM+	4654	4877
	PAN _ OLI	2932	3056
Iranshahr	PAN _ ETM+	3462	3308
	PAN _ OLI	2693	2521

The PCA image for each dataset was rendered using ETM+ bands 1 to 5, and 7, and OLI bands 1 to 7, and 9, respectively. The results for execution of LINE algorithm on PC1 image derived from ETM+ and OLI datasets are tabulated in Table 2. The data indicate that in all of the study areas except for one study area (i.e. Rafsanjan study area), the LINE algorithm performed more satisfactorily on PC1 image derived from ETM+ dataset compared to PC1 image derived from OLI dataset.

Table 2. Results of execution the Line algorithm on PC1 images of ETM+ (8-bit depth) and OLI (16-bit depth) datasets.

Field study	Data type	Number of segments	Sum of lengths (km)
Shahrekord	PAN _ ETM+	2757	4547
	PAN _ OLI	2266	3459
Tabriz	PAN _ ETM+	1427	2414
	PAN _ OLI	1414	2399
Larestan	PAN _ ETM+	1188	2331
	PAN _ OLI	902	1665
Iranshahr	PAN _ ETM+	744	1154
	PAN _ OLI	600	929

The LINE algorithm converts any input image to an 8-bit image by a nonlinear function before linear feature detection. This is true for OLI data which is in 16 bits. To investigate the effect of this conversion on the outcome of LINE algorithm, the OLI images used for all study areas were converted to 8-bit images with both linear and nonlinear logarithmic functions before execution of LINE algorithm using Equations (2) and (3). Figure 4 shows the histograms of one of the study areas of original OLI image and the converted versions of it to 8-bit with two mentioned functions. The results of LINE algorithm, on both types of converted images for each study area, are tabulated in Table 3.

Table 3. Results of LINE algorithm on the panchromatic bands and PC1 images of converted 16 to 8-bit OLI using both linear and nonlinear (logarithmic) functions and 8-bit originally ETM+

Field study	Data type	OLI converted by Logarithmic function		OLI converted by the Linear function	
		Sum of segments	Sum of lengths (km)	Sum of segments	Sum of lengths (km)
Shahrekord	PAN _ ETM+	9604	9534	9604	9534
	PC1 _ ETM+	2757	4547	2757	4547
	PAN _ OLI	7297	6780	7158	6672
	PC1 _ OLI	2126	3302	2084	3225
Tabriz	PAN _ ETM+	5046	5047	5046	5047

	PC1 _ ETM+	1427	2414	1427	2414
	PAN _ OLI	3735	3660	3656	3575
	PC1 _ OLI	1391	2345	1363	2309
	PAN _ ETM+	4654	4877	4654	4877
Larestan	PC1 _ ETM+	1188	2331	1188	2331
	PAN _ OLI	2786	2843	2753	2828
	PC1 _ OLI	898	1665	879	1640
	PAN _ ETM+	3462	3308	3462	3308
Iranshahr	PC1 _ ETM+	744	1154	744	1154
	PAN _ OLI	2744	2573	2619	2459
	PC1 _ OLI	607	940	567	892
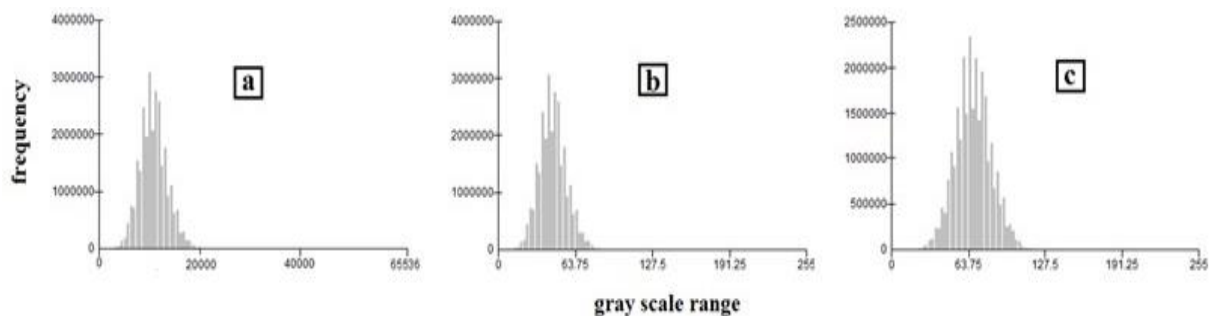
Figure 4. Histograms of the transformed OLI image from 16 to 8-bit depth for Yasuj; (a): original 16-bit image; (b): converted using linear function; and (c): converted using logarithmic function.

Comparison of the standard deviations of all images in Table 4, including PC1 and panchromatic band after normalization by Equation (5) shows that logarithmic function always produced images with higher standard deviations compared to images converted by a linear function. Standard deviation is a measure of the spread of values around the mean. Lower the standard deviation more the values is clustered around the average. Standard deviation is a useful measure of image contrast. An image with a higher standard deviation shows higher contrast [21].

Table 4. Standard deviation of compared images.

Study Field	Panchromatic band				PC1 image			
	Original		OLI converted to 8-bit		Original		OLI converted to 8-bit	
	ETM+	OLI	Linear	Logarithmic	ETM+	OLI	Linear	Logarithmic
Yasuj	0.072	0.037	0.037	0.052	0.088	0.047	0.048	0.062
Yazd	0.075	0.043	0.043	0.057	0.097	0.075	0.076	0.085
Rafsanjan	0.063	0.053	0.053	0.056	0.061	0.083	0.083	0.091
Shahrekord	0.084	0.030	0.030	0.042	0.101	0.036	0.037	0.048
Mashhad	0.095	0.060	0.060	0.079	0.095	0.090	0.091	0.093
Tabriz	0.049	0.027	0.027	0.042	0.077	0.063	0.063	0.073
Larestan	0.103	0.092	0.093	0.095	0.112	0.096	0.093	0.097
Iranshahr	0.077	0.050	0.051	0.063	0.084	0.058	0.058	0.069

In all cases, the LINE algorithm gave better results on the image pair which was converted using a logarithmic function rather than the one converted by a linear function. However, execution of the LINE algorithm on 8-bit converted OLI images always gave poorer results compared to ETM+ 8-bit images. The LINE algorithm always performed better on image pairs which had a higher standard deviation (Tables 2, 3 and 4). This is the case for both panchromatic bands and PC1 images. The OLI PC1 image of the exceptional study area (i.e. Rafsanjan city) for which OLI PC1 image gave better results in LINE algorithm had higher standard deviation compared to ETM+ PC1 image. There seems to be more secured

information for LINE algorithm in images with the higher standard deviation in each study area. The higher standard deviation of ETM+ bands is most probably a result of broader bandwidth of ETM+ sensor relative to the OLI sensor. The panchromatic band of the ETM+ sensor is 0.208 micrometers wider than the panchromatic band of OLI. Additionally, other bands of ETM+ sensor which record data in the reflective region of the electromagnetic spectrum are about 0.32 micrometers wider than the corresponding OLI bands. A band with wider spectral region contains more information reflected from the earth surface. When the goal is the detection of the linear phenomenon, a wider bandwidth seems to be more efficient because the edge can be composed of various materials with various spectral features. This is contrary to the usefulness of narrower bandwidths for the detection of specific spectral materials [22].Therefore, when detecting linear features by LINE algorithm, ETM+ images with higher spectral bandwidth are preferred over OLI images.

5. Conclusion

The LINE algorithm is the fastest and most efficient method for linear feature extraction. The resolving power of the sensor and its spatial resolution, and the bandwidth of the sensor are influential factors in linear feature detection. Images with higher standard deviation have higher contrast and give better results for linear feature extraction by LINE algorithm. Because standard deviation and image contrast are directly related to the spectral bandwidth of the sensor, the images recorded in wider spectral bandwidth are more suitable for linear feature extraction. It was shown that ETM+ panchromatic and PC1 bands almost always have higher standard deviation compared to panchromatic and PC1 bands of OLI datasets. Therefore, ETM+ datasets with higher bandwidth are more favourable for the linear feature extraction compared to OLI datasets.

References

[1]   Al-Nahmi F, Alami O B, Baidder L, Khanbari K, Rhinane H, Hilali A, 2016, Using remote sensing for lineament extraction in al-Maghrabah area, Hajjah, Yemen. *The International Archives of Photogrammetry, Remote Sensing and Spatial Information Sciences*, **42**, 137.

[2]   Imanian A, Sheykhi V, Zare K, Zare M, 2020, Introducing the recharge–discharge relationship to evaluate the recharge coefficient of karstic aquifers: thematic and indexing approaches, *Hydrological Sciences Journal*, **65**:8, 1385-1398, DOI: 10.1080/02626667.2020.1739288.

[3]   Imanian A, Tangestani M H, Asadi A, 2019, Investigation of spectral characteristics of carbonate rocks – a case study on posht moleh mount in Iran, *Int. Arch. Photogramm. Remote Sens. Spatial Inf. Sci.*, XLII-4/W18, 553–557, International Society for Photogrammetry and Remote Sensing. https://doi.org/10.5194/isprs-archives-XLII-4-W18-553-2019, 2019.

[4]   Imanian A, Tangestani M H, Asadi A, 2019, Investigation of spectral characteristics of carbonate rocks – a case study on Posht Moleh mount in Iran, *Int. Arch. Photogramm. Remote Sens. Spatial Inf*. Sci., XLII-4/W18, 553–557, International Society for Photogrammetry and Remote Sensing. https://doi.org/10.5194/isprs-archives-XLII-4-W18-553-2019, 2019.

[5]   Rostamijavanani A, Ebrahimi M R, Jahedi S, 2021, Thermal post-buckling analysis of laminated composite plates embedded with shape memory alloy fibers using semi-analytical finite strip method. *J Fail. Anal. and Preven.* **21,** 290–301 (2021). https://doi.org/10.1007/s11668-020-01068-5.

[6]   Khaleghi H, Farani Sani H, Ahmadi M, Mohammadzadeh F, 2021, Effects of turbulence on the secondary breakup of droplets in diesel fuel sprays. Proceedings of the Institution of Mechanical Engineers, Part D: *Journal of Automobile Engineering*, 235(2–3), 387–399. https://doi.org/10.1177/0954407020958581.

[7]   Hui F, Li X, Zhao T, Shokr M, Heil P, Zhao J, Cheng X, 2016. Semi-automatic mapping of tidal cracks in the fast ice region near Zhongshan station in East Antarctica using Landsat-8 OLI imagery. *Remote Sensing*, **8**(3), 242.

[8]   Asadi A, 2015, Application of artificial neural networks in estimation of uniaxial compressive strength using Schmidt hammer rebound number data under specific geological conditions, Paper

presented at the *ISRM Regional Symposium - EUROCK 2015*, Salzburg, Austria, October 2015. ISRM-EUROCK-2015-177, ISBN: 978-3-9503898-1-4.

[9]   Rashidi M., Asadi A, Biltayib B M, 2019, Correlation between uniaxial compressive and shear strength data of limestone rocks by regression analysis and ANFIS model. In: Kallel A. et al. (eds) *Recent Advances in Geo-Environmental Engineering, Geomechanics and Geotechnics, and Geohazards*. CAJG 2018. Advances in Science, Technology & Innovation (IEREK Interdisciplinary Series for Sustainable Development), Springer. https://doi.org/10.1007/978-3-030-01665-4_39.

[10]   Canny J F, 1987, A computational approach to edge detection, Readings in computer vision: issues, problems, principles, and paradigms. *IEEE Trans. Pattern*.

[11]   Ghorbani M, 2013, A summary of geology of Iran. In: *The Economic Geology of Iran* (pp. 45-64). Springer, Dordrecht.

[12]   Nabavi M H, 1976, An introduction to the geology of Iran, *Geological Survey of Iran.*

[13]   Rashidi M, Hajipour M, Asadi A, 2018, Correlation between static and dynamic elastic modulus of limestone formations using artificial neural networks, Paper presented at the 52nd U.S. Rock Mechanics/Geomechanics Symposium, Seattle, Washington, June 2018. ARMA-2018-247.

[14]   Rostamijavanani A, Dynamic buckling of cylindrical composite panels under axial compressions and lateral external pressures. *J Fail. Anal. and Preven.* **21,** 97–106 (2021). https://doi.org/10.1007/s11668-020-01032-3.

[15]   Haryono E, Widartono B, Lukito H, Kusumayuda S B, 2016, A comparison of lineament and fracture trace extraction from Landsat ETM+ panchromatic band and panchromatic aerial photograph in Gunungsewu karst area, Java-Indonesia. In: *IOP Conference Series: Earth and Environmental Science* (Vol. **47**, No. 1, p. 012026). IOP Publishing.

[16]   Chrysoulakis N, Abrams M, Feidas H, Arai K, 2010, Comparison of atmospheric correction methods using ASTER data for the area of Crete, Greece. *International Journal of Remote Sensing*, **31**(24), 6347-6385.

[17]   Khameneian A, Wang X, Dice P, Shahbakhti M, Naber J D, Archer C, Moilanen P, Glugla C, Huberts G, 2020, Model-based dynamic in-cylinder air charge, residual gas and temperature estimation for a GDI spark ignition engine using cylinder, intake and exhaust pressures, *Proceedings of the ASME 2020 Dynamic Systems and Control Conference*. October 5–7, 2020. V002T26A002. https://doi.org/10.1115/DSCC2020-3280.

[18]   Ahmadi B, Talesh Bahrami H R, Saffari H.; 2016, Production of superhydrophobic copper surfaces by fabricating micro-nano features using wet etching process. Modares Mechanical Engineering. 2016; 16 (5) :389-395; URL: http://mme.modares.ac.ir/article-15-10885-en.html.

[19]   Richards J A, 2013, *Remote sensing digital image analysis* (5th edition). Springer.

[20]   Talesh Bahrami H R, Ahmadi B, Saffari H, 2017, Optimal condition for fabricating superhydrophobic copper surfaces with controlled oxidation and modification processes, *Materials Letters*, Volume **189**, 2017, Pages 62-65, ISSN 0167-577X, https://doi.org/10.1016/j.matlet.2016.11.076.

[21]   Gonzalez R C, Woods R E, 2002, *Digital image processing*, second edition. Beijing: Publishing House of Electronics Industry, 455.

[22]   Adams J B, Gillespie A R, 2006, *Remote sensing of landscapes with spectral images: A physical modeling approach*, Cambridge University Press.